ACS APPLIED MATERIALS & INTERFACES

Research Article

www.acsami.org

Magnetic-Assembly Mechanism of Superparamagneto-Plasmonic Nanoparticles on a Charged Surface

Van Tan Tran,[†,‡] Hongjian Zhou,[‡,§] Seunghun Lee,[†] Seong Cheol Hong,[†] Jeonghyo Kim,[†] Se-Young Jeong,[†] and Jaebeom Lee*[,†]

[†]Department of Cogno-Mechatronics Engineering, Pusan National University, Busan 609-735, Republic of Korea

[§]Key Laboratory of Materials Physics, Centre for Environmental and Energy Nanomaterials, Anhui Key Laboratory of Nanomaterials and Nanotechnology, Institute of Solid State Physics, Chinese Academy of Sciences, Hefei 230031, P. R. China

Supporting Information

ABSTRACT: One-dimensional magnetoplasmonic nanochains (MPNCs) were self-assembled using Au-coated Fe_3O_4 core–shell superparamagnetic nanoparticles (Fe_3O_4@Au NPs) by applying an external static magnetic field. The assembly mechanism of the Fe_3O_4@Au NPs was investigated thoroughly, revealing that substrate–particle interactions, van der Waals forces, and magnetic forces play important roles in the formation and control of the MPNCs. Magnetic force microscopy (MFM) and vibrating sample magnetometry (VSM) were used to study the magnetic properties of the MPNCs, which were compared with those of Fe_3O_4 nanochains.

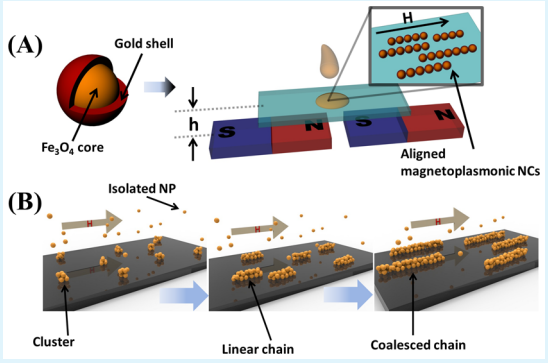

KEYWORDS: *Fe_3O_4@Au, core–shell nanoparticle, self-assembly, magnetoplasmonic nanoparticle, nanochain*

1. INTRODUCTION

One-dimensional (1D) magnetic nanomaterials have recently received attention because of their unique magnetic characteristics.[1] In nature, 1D magnetic structures have been found in magnetotactic bacteria and magnetoception of animals. The arrangement of biogenic ferrimagnetic materials, typically magnetite, into chains is believed to aid organisms in reaching regions of optimal oxygen concentration in the case of bacteria or detecting a magnetic field to perceive direction, altitude, or location in the case of animals.[2,3] Such 1D magnetic structures are fabricated using various materials and different techniques. Much effort has been put forth to reveal the assembly mechanism in biogenic and synthetic systems.[4,5] In living entities, the assembly mechanism involves a combination of physical (magnetic)[6] and molecular (genetic)[7] processes. Detailed studies of physical assembly processes of synthetic nanoparticles (NPs) generally demonstrated that two major types of forces, namely, van der Waals (vdW) and magnetic dipole forces, are exerted on magnetic NPs dispersed in solution.[8] For high-magnetic-moment NPs (e.g., single-domain magnetite NPs in a magnetosome), the strength of the dipole moments controls the formation of chainlike structures of individual NPs.[9,10] However, for sufficiently small NPs, typically superparamagnetic single-crystal magnetite NPs, the value of magnetic moment is too small to produce significant dipolar interactions. Therefore, vdW interactions are expected to be the dominant contribution to the total interparticle potential.[11] Clear evidence was seen in the upper-beak skin of homing pigeons in which aggregates of magnetite NPs (with grain sizes between 1 and 5 nm) are arranged in coherent elongated structures.[12,13] In addition to the two above-mentioned forces, the interactions between the substrate and the particles are not negligible, especially in evaporating solutions, where out-of-equilibrium states, which depend on the balance between interparticle forces, the substrate–particle interactions, and the flow induced in the evaporating droplet, prevail.[14]

The effect of coating a gold shell onto Fe_3O_4 NPs is attractive to investigate.[15] The incorporation of a gold layer on a magnetic core provides unique plasmonic and electrical properties to the material.[16] Additionally, it is believed that the Au coating not only acts as a barrier protecting the NPs against external agents but also modifies the magnetic properties by isolating the magnetic cores or by interface coupling interactions.[17,18] Consequently, the 1D assembly of these core–shell NPs could give rise to novel and unexpected magnetic properties. This could result in highly promising applications of such core–shell NPs in multilmodal imaging and photomagnetic therapy and of the magnetoplasmonic nanochains in waveguides, antennas, magnetoresistance, and so on. Furthermore, the Au metal coated on the surface of magnetic NPs endows the magnetoplasmonic nanochains (MPNCs) with excellent conductivity. Based on this novel

Received: January 30, 2015
Accepted: April 9, 2015
Published: April 9, 2015

DOI: 10.1021/acsami.5b00904
ACS Appl. Mater. Interfaces 2015, 7, 8650–8658

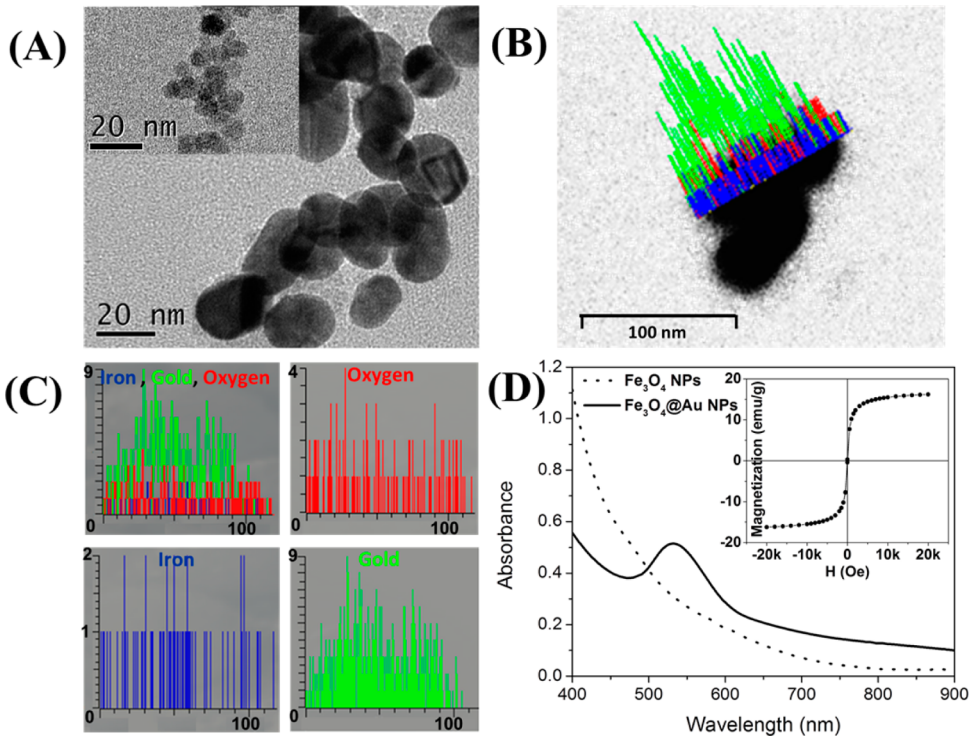

Figure 1. (A) TEM images of Fe_3O_4@Au NPs and bare Fe_3O_4 NPs (inset). (B) Elemental mapping line scans of Fe_3O_4@Au NPs for O (red), Fe (blue), and Au (green), superimposed on the TEM image. (C) Overlapped and separated elemental mapping line scans of Fe_3O_4@Au NPs for each element. (D) UV−vis curves of Fe_3O_4 and Fe_3O_4@Au NPs and room-temperature magnetization curve of Fe_3O_4@Au NPs (inset).

property, we recently reported an electrical biosensor for the rapid and label-free detection of DNA.[16]

In this work, we investigated the assembly mechanism and magnetic properties of the nanochains. Integration of a Au layer onto Fe_3O_4 NPs not only introduces novel properties to corresponding assembled structures but also modulates the magnetic behavior of the collection of particles, resulting in unforeseen properties. The results presented here support the observation of assembled Fe_3O_4@Au NPs and suggest the possibility of using such a mechanism to construct and regulate other assembled structures consisting of nanoscale building blocks.

2. EXPERIMENTAL SECTION

2.1. Materials. Hydrogen tetrachloroaurate(III) trihydrate ($HAuCl_4{\cdot}3H_2O$, 99.9%), sodium citrate ($Na_3C_6H_5O_7$), $FeCl_3{\cdot}6H_2O$, were obtained from Sigma-Aldrich Korea Ltd. (Yong-In, South Korea). $FeCl_2{\cdot}4H_2O$ was purchased from Wako Pure Chemical Industries Ltd. (Osaka, Japan). Ammonia solution (28% w/v) was procured from Duksan Pure Chemical Co., Ltd. (Gyeonggi, South Korea). Deionized H_2O (18.2 mΩ/cm) that was used in most experiments was obtained from Human Corporation (Seoul, South Korea). All chemicals were of analytical grade and were used as received.

2.2. Synthesis of Fe_3O_4 and Fe_3O_4@Au NPs. Fe_3O_4 and Fe_3O_4@Au NPs were synthesized according to our previously reported method.[19] Briefly, to synthesize Fe_3O_4 NPs, 1.622 g of $FeCl_3{\cdot}6H_2O$ and 0.9941 g of $FeCl_2{\cdot}4H_2O$ were dissolved in 40 mL of water, accompanied by constant mechanical stirring. A total of 5 mL of ammonia solution (28% w/v) was added to the completely dissolved reaction mixture, and the resulting mixture was allowed to stand for 10 min. Then, 4.4 g of sodium citrate was added, and the reaction temperature was raised to 90 °C. Under continuous stirring, this reaction was carried out for 30 min. A black precipitate was obtained by cooling the reaction mixture to room temperature. The precipitate was then thoroughly rinsed with copious amounts of water.

For the preparation of Fe_3O_4@Au NPs, 20 mL of 0.5 mM $HAuCl_4$ solution was heated and stirred vigorously until it boiled. Rapid addition of 10 mL of the Fe_3O_4 NPs solution prepared in the previous step (approximately 0.136 μM in NPs) resulted in a continuous color change of the solution from brown to burgundy. The solution was stirred for 15 min, after which the heating source was removed. Stirring was continued until the solution cooled to room temperature. The resulting solution was then centrifuged three times at 5000 rpm for 30 min to remove free Fe_3O_4 NPs. After that, a permanent magnet was used to separate pure Au NPs. The final solution was stored at 4 °C until further use.

2.3. Preparation of 1D Alignment of Fe_3O_4@Au NPs. An external magnetic field was utilized to prepare 1D magnetoplasmonic NCs (MPNCs) using Fe_3O_4@Au NPs; the prepared NPs were directionally aligned using neodymium (NdFeB) block magnets (20 mm × 10 mm × 5 mm) (Figure 1A). Typically, a drop (14 μL) of the colloidal dispersion was dropped onto glass substrate (18 × 18 mm, Matsunami Glass Inc., Osaka, Japan) that was located above the center point between two magnets, hence assuring a uniform field at this position. The setup was kept undisturbed at a certain temperature until the colloidal suspension had completely dried.

2.4. Molecular Dynamics Simulation of 1D Assembled Fe_3O_4@Au Nanostructures. Molecular dynamics simulations of 1D assembled Fe_3O_4@Au nanostructures were carried out on a layer slab structure with periodic boundary conditions at different temperatures. The simulations were conducted with Materials Studio (v4.2 package, Accelrys, San Diego, CA) using condensed-phase optimized molecule potentials for atomistic simulation studies (COMPASS) force fields. The space group of Au is *Fm*3*m*, and its lattice parameters are $a = b = c = 4.0782$ Å and $\alpha = \beta = \gamma = 90°$, which are very similar to those reported in the literature. Comparisons validated the applicability of the COMPASS force fields to the Au−Fe_3O_4 crystal structure simulation. The surface of the Fe_3O_4@Au NPs was built by cleaving along the (111) planes of Au and then using the smart minimizer method under periodic boundary conditions with a nonbonded cutoff distance of 9.5 Å.

DOI: 10.1021/acsami.5b00904
ACS Appl. Mater. Interfaces 2015, 7, 8650−8658

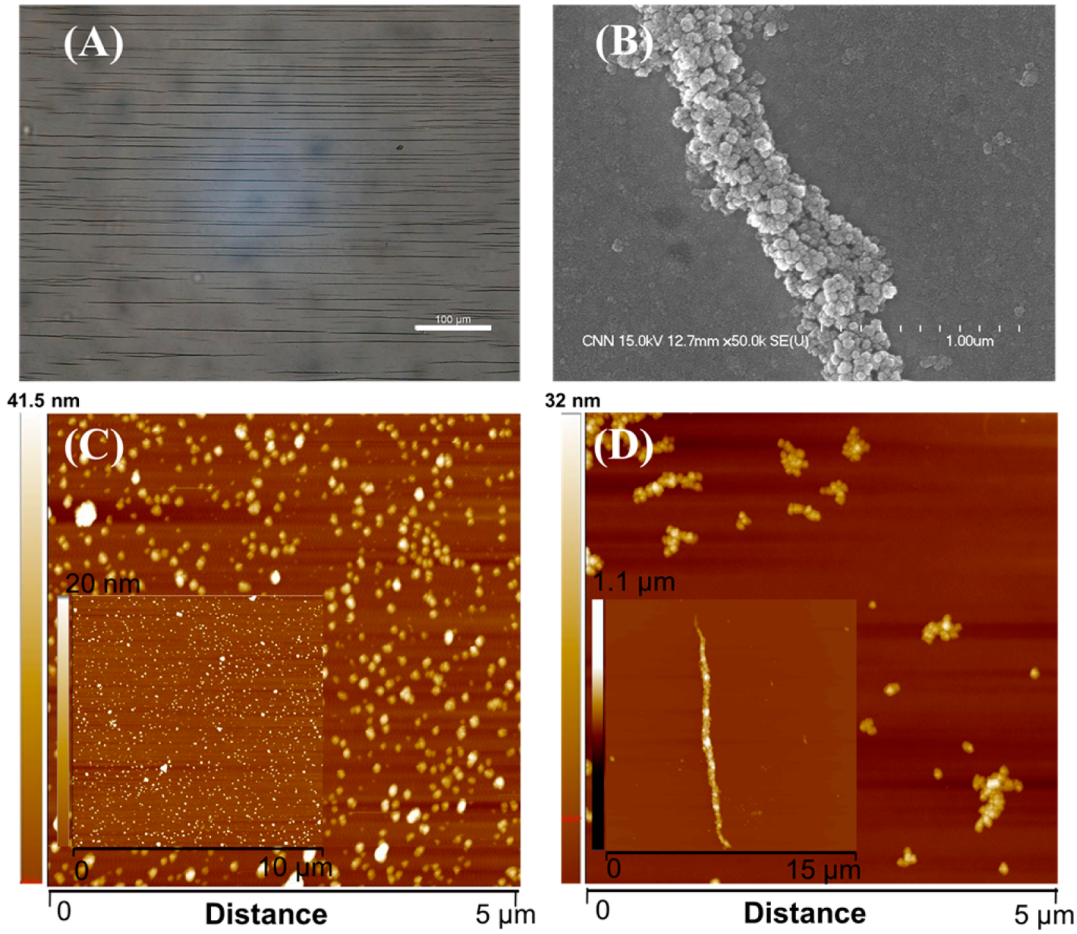

Figure 2. (A) Optical microscopy and (B) SEM images of MPNCs. AFM images of Fe_3O_4@Au core−shell NP assemblies: (C) on a poly(diallyldimethylammonium chloride)- (PDDA-) modified glass without and (inset) with an applied magnetic field and (D) on a bare glass without and (inset) with an applied magnetic field.

2.5. Characterization. The absorbance of Fe_3O_4@Au NPs was measured by UV−vis spectroscopy (S310, Scinco, Seoul, South Korea), whereas the chemical reactions were monitored by Fourier transform infrared (FT-IR) spectroscopy (FTIR6300, JASCO, Tokyo, Japan). The morphologies, sizes, and magnetic properties of the Fe_3O_4@AuNPs and MPNCs were characterized by high-resolution transmission electron microscopy (HR-TEM) (JEM-3010, JEOL, Tokyo, Japan), field-emission scanning electron microscopy (FE-SEM) (S-4700, Hitachi, Tokyo, Japan), optical microscopy (DM2000, Leica, Wetzlar, Germany), atomic force microscopy (AFM), and magnetic force microscopy (MFM) (Innova, Veeco, Plainview, NY). Furthermore, their surface potentials and particle size distributions were monitored using a Zetasizer (ZS Nano, Malvern Instruments, Malvern, U.K.). Magnetic measurements were performed using a superconducting quantum interference device (SQUID) magnetometer (MPMS XL-7, Quantum Design, Inc., San Diego, CA). The field- and temperature-dependent magnetizations of the NPs and NCs were measured by vibrating sample magnetometry (VSM) (model 6000, Quantum Design, Inc., San Diego, CA). Zero-field-cooled (ZFC) and field-cooled (FC) measurements were acquired using an applied field of 100 Oe between temperatures of 10 and 300 K in discrete steps of 10 K. The field-dependent magnetization was collected within ±20 kOe at both 300 and 10 K. To exclude other magnetic contributions, special care was taken during the sample transferring and holding process; diamagnetic contributions from the SiO_2 substrate and the holding system were preliminarily confirmed and mathematically subtracted. Normalization with respect to the saturation magnetization was performed for comparative purposes, suppressing any quantitative effects.

3. RESULTS AND DISCUSSION

3.1. Characterization of Fe_3O_4@Au NPs. Fe_3O_4@Au core−shell NPs were synthesized in an aqueous solution through the reduction of $HAuCl_4$ using Fe_3O_4 NPs as seeds. Figure 1A shows TEM images of Fe_3O_4@Au NPs and bare Fe_3O_4 NPs. The average sizes of the Fe_3O_4@Au NPs and bare Fe_3O_4 NPs were about 20 and 10 nm, respectively. The thickness of the Au shell was therefore estimated to be around 5 nm. The core−shell structure of the Fe_3O_4−Au NPs was verified by X-ray diffraction (XRD), as reported previously.[20] Here, we performed an elemental mapping analysis of Fe, Au, and O present in the NPs (Figure 1B,C). The elemental mapping images were obtained by energy-dispersive X-ray (EDX) spectroscopy. The line-scanning analysis clearly showed the spatial distributions of the elements according to the core−shell structure. It was observed that the Au shell exhibited the most intense uniform line, which can be attributed to the fact that the density of Au surface electrons was higher than those of Fe and O surface electrons. By superimposing the elemental mapping images over the TEM image (Figure 1B), we confirmed that the locations of the Au shell and Fe_3O_4 core matched exactly with the expected nanostructure, indicating that the shell and core were composed of Au and Fe_3O_4, respectively. The magnetic properties of Fe_3O_4@Au NPs were examined at room temperature, and the results are shown in the inset of Figure 1D. The hysteresis loop indicates super-

DOI: 10.1021/acsami.5b00904
ACS Appl. Mater. Interfaces 2015, 7, 8650−8658

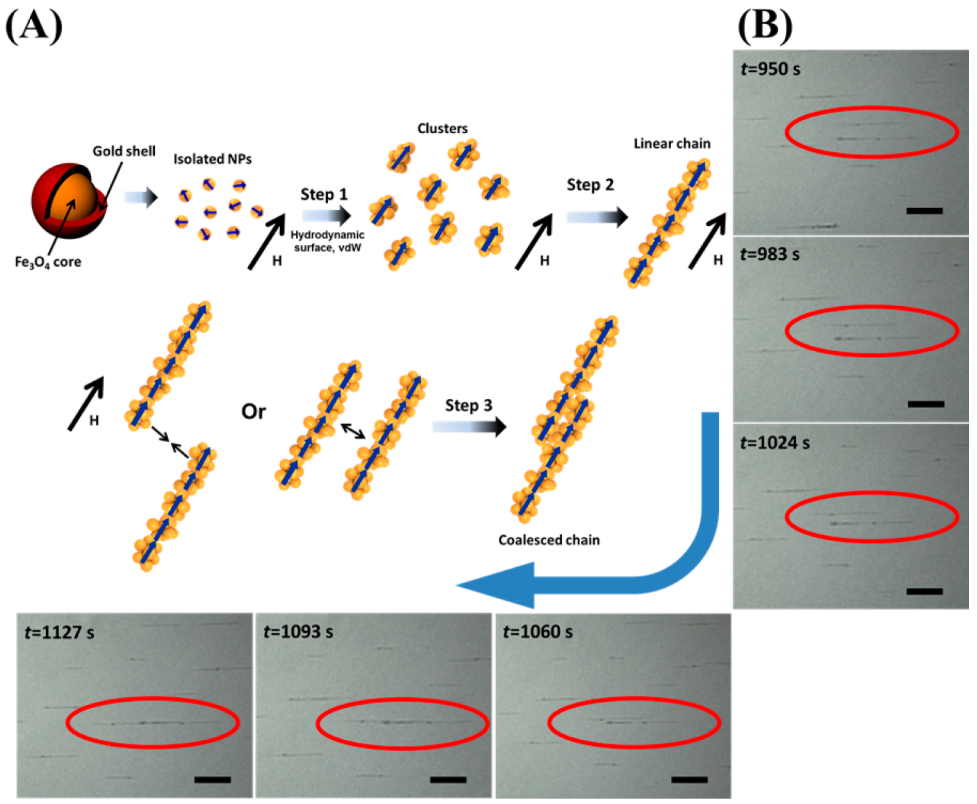

Figure 3. (A) Schematic illustration of the structure of Fe_3O_4@Au NPs and the assembly mechanism of NPs into magnetoplasmonic nanochains. (B) Sequence of microscope images of a typical arrangement of NCs from side-to-side to head-to-tail configuration. Scale bars = 25 μm.

paramagnetism of the core−shell NPs at room temperature, whereas the saturation magnetization decreased to 16.2 emu g^{-1} from a value of 66.8 emu g^{-1} for the Fe_3O_4 NPs.[20] This reduction is believed to be due to the increased interparticle spacing of the magnetic cores that results in a decreased coupling of the magnetic moments for the Au-coated surfaces (in the powder state).[21] UV−vis absorption spectra of Fe_3O_4 and Fe_3O_4@Au NPs are shown in Figure 1D. These spectra provide indirect evidence supporting the formation of the Fe_3O_4@Au core−shell morphology. The Fe_3O_4 NPs exhibited no measurable features in the visible region; however, a plasmon absorption peak at 532 nm was observed for the Fe_3O_4@Au NPs, indicating the presence of a Au shell. The observed red shift and peak broadening when compared to the spectrum of pure spherical Au NPs of similar size (absorption peak at 520 nm for 3−20-nm Au NPs[22]) are caused by the interaction of "primitive" plasmons associated with the inner (cavity plasmons) and outer (sphere plasmons) surfaces of the Au shells around the Fe_3O_4 cores and a deficient electron population in the Au shell due to interaction of both plasmon types.[23,24]

3.2. Magnetic Assembly Mechanism of Superparamagneto-Plasmonic NPs. Assemblies of Fe_3O_4@Au NPs (10 μg mL^{-1}) on a glass substrate in an external magnetic field (**B** $\approx$ 20 mT) parallel to the plane of the sample at 35 °C are shown in Figure 2A,B. On the microscale, the NPs are assembled along the direction of the externally applied magnetic field, exhibiting lengths of hundreds of microns and widths of less than 1 μm. However, on the nanoscale, randomly aggregated NPs are composed of MPNCs, as shown in Figure 2B.

In ferrofluid systems, the formation of particles into chains is likely to occur only if the magnetic forces can overcome the thermal forces. A dipolar solid will occur if the magnetic dipolar parameter χ is greater than 3 [see the Supporting Information (SI)], in which thermal forces are small compared to the magnetic forces. In the opposite limit (χ < 3), structure formation is unlikely, and the magnetic field can be treated as a small perturbation.[8,25] The magnetic dipolar parameter χ was estimated to have values of ~2.96 and ~0.37 for our Fe_3O_4 and Fe_3O_4@Au NPs, respectively (see SI), which indicates that the magnetic dipolar energies of the individual bare and core−shell NPs were not sufficiently strong to induce chain formation at room temperature.[26,27] Therefore, the role of vdW forces among the magnetic NPs needs to be considered to explain the formation of MPNCs in a magnetic field, even in a system in which dipolar interactions are low compared to the thermal energy.

A theory proposed by Pileni et al.[8] confirmed the role of vdW forces using magnetic NPs with coating layers of different thicknesses. They concluded that, because of the van der Waals interactions, when the coating molecule was short enough, clusters of nanocrystals formed during the evaporation process. By using cyro-TEM, in which an extremely high cooling rate is applied to keep the original state of NPs in solution, they observed a cluster structure of nanocrystals under zero field when the isotropic van der Waals attraction contributed significantly.[28] It is plausible that cluster formation can enhance long-range dipolar forces, as the magnetic moment of an NP cluster is equal to the sum of the magnetic moments of each individual NP.[8,11,28,29] Notice that electrostatic and/or steric repulsions between NPs have to be relatively weak so that vdW force can overcome opposing forces[30,31] to successfully align

DOI: 10.1021/acsami.5b00904
ACS Appl. Mater. Interfaces 2015, 7, 8650−8658

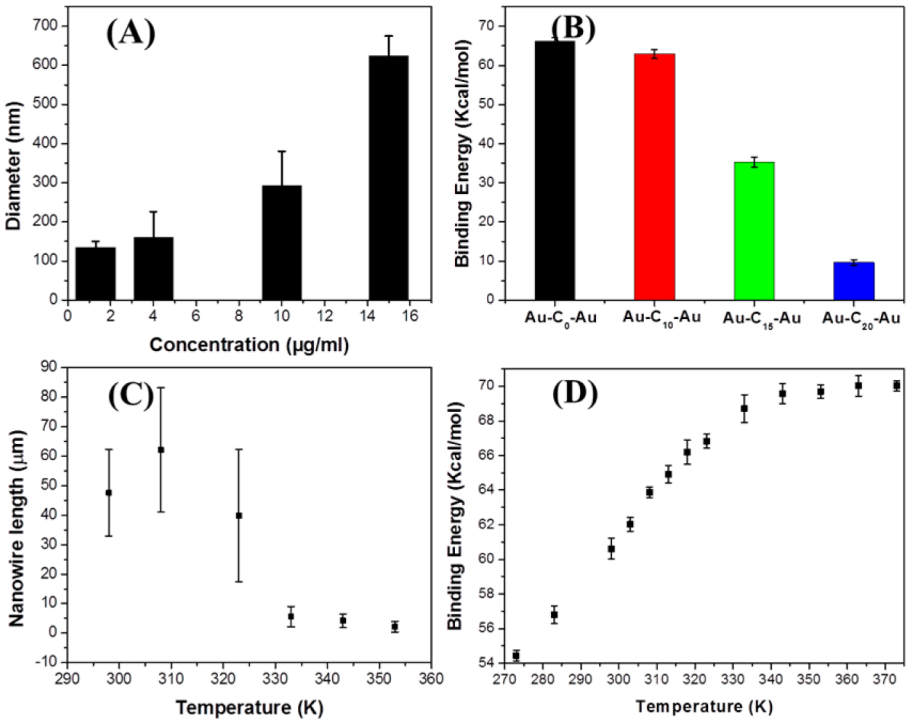

Figure 4. (A,C) Dependence of the MPNC (A) diameter and (C) length on the colloidal concentration and (B,D) calculated binding energies between two Fe_3O_4@Au NPs as a function of (B) interparticle distance and (D) temperature.

superparamagnetic NPs into 1D structures along the magnetic field direction. Interestingly, we experimentally found that chains of both bare Fe_3O_4 and Fe_3O_4@Au NPs could not be observed in bulk solution (discussed below). This reveals that another force associated with the flat surface of the substrate could also contribute in governing the assembly of NPs whose magnetic moments are not large enough to individually produce significant dipolar interactions.

For like-charged particles, the established Derjaguin–Landau–Verwey–Overbeek (DLVO) theory predicts that the pairwise interaction of two isolated identically charged particles is a purely repulsive one.[32,33] However, experimental and theoretical studies have confirmed the existence of a long-range attraction between identically charged colloidal particles that are immersed in an electrolyte or in confined geometries.[34−36] Theoretical explanations that have been proposed include the electrostatic influence of confining surfaces, solvation effects,[36] osmotically driven processes,[37] and hydrodynamic effects.[38] We performed experiments on glass substrates with different surface charges to investigate the mechanism of cluster formation. Figure 2C,D shows assembled structures of core–shell NPs on different flat surfaces in the absence of a magnetic field. In the case of a poly(diallyldimethylammonium chloride)- (PDDA-) coated glass surface [zeta potential (ζ) ≈ +55 mV at neutral pH[39]], isolated core–shell NPs, which have negatively charged surfaces because of their stabilizing layer, are homogeneously distributed. In contrast, many large clusters are formed on a bare glass surface, which has a negative charge ($\zeta \approx -30$ mV[40]). Clusters with varying shapes consist of a few to several tens of single core–shell NPs (Figure 2C). Experiments employing poly(acrylic acid)- (PAA-) modified glass ($\zeta \approx -58$ mV[40]) provide results similar to those obtained with the bare glass (results not shown). Differences between the resulting structures on positively and negatively charged surfaces upon application of a magnetic field are even more striking (insets of Figure 2C,D). The morphology of the core–shell NP assembly on the PDDA-modified glass is the same when subjected to a magnetic field as when under zero-field conditions: Isolated core–shell NPs are randomly dispersed, and there is no sign of long-range dipolar interactions. However, in the case of the bare glass, 1D oriented chains are observed in the presence of a magnetic field. Similar results were obtained using bare Fe_3O_4 NPs as well (result not shown). According to theoretical calculations reported in Table S1 (SI), the average magnetic dipolar parameters (χ) of clusters of bare Fe_3O_4 and Fe_3O_4@Au were estimated to be 38 and 5, respectively, which are greater than the threshold ($\chi = 3$) for chain formation. More investigation of the assembly processes of MPNCs using live recording microscopy not only provides detailed information about MPNC growth, but also confirms the aforementioned reasoning. As expected, no NCs can be observed in the bulk solution or on the PDDA-modified glass surface (see Video 1, SI). In the case of the bare glass, NCs are observed on the surface but not in the bulk solution (see Video 2, SI). These result reconfirms that cluster formation occurs only near flat surfaces that are either neutral or negatively charged ($\zeta < 0$) and that the magnetic dipolar interaction of isolated NPs that exists in both bulk solutions and on positive flat surfaces ($\zeta > 0$) is not sufficient to overcome the thermal energy and arrange the NPs into anisotropic structures.

In our system, the assembly process of MPNCs can be divided into three steps, as shown in Figure 3A: (1) cluster formation of NPs, (2) cluster–cluster chaining, and (3) consecutive chain–chain aggregation. Cluster formation of magnetic NPs can be attributed to the interactions between the NPs and the charged surface. In the case of the positively charged PDDA-modified surface, the strong electrostatic attraction between the NPs and the surface could overwhelm any other interactions. Nanoparticles near the surface, which are strongly attracted to the substrate, do not participate in the

DOI: 10.1021/acsami.5b00904
ACS Appl. Mater. Interfaces 2015, 7, 8650−8658

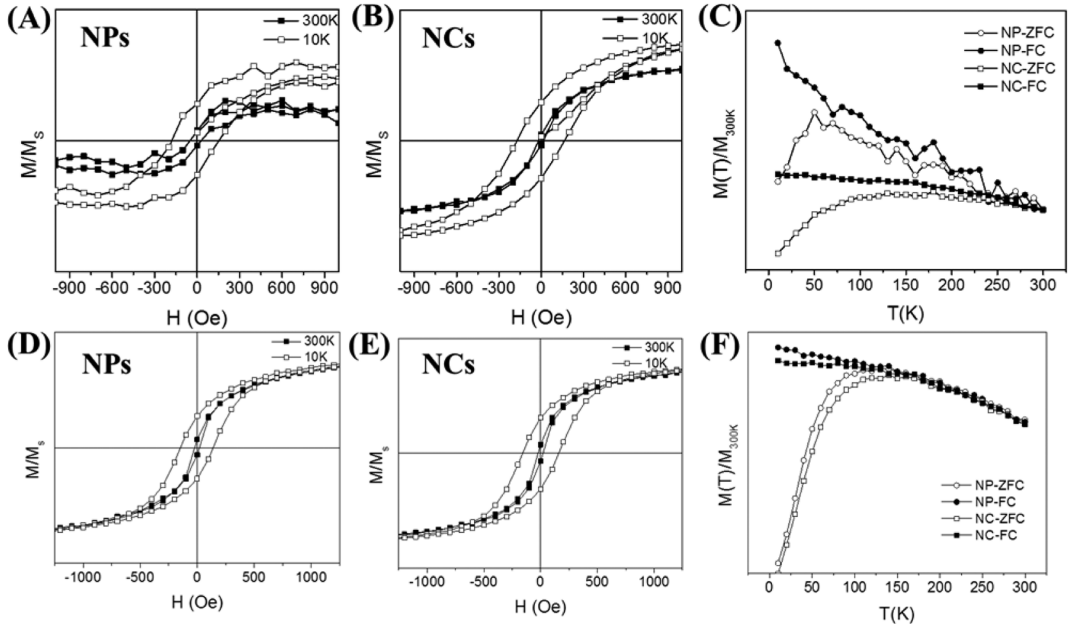

Figure 5. Hysteresis loops of (A) bare Fe_3O_4 NPs and (D) Fe_3O_4@Au NPs and (B,E) their corresponding NCs at 300 and 10 K. (C,F) Temperature-dependent magnetizations of NPs and their corresponding NCs: (C) bare Fe_3O_4 and (F) Fe_3O_4@Au NPs.

assembly process. Because the nanoparticles are not immediately attracted to the positive surface, suspended nanoparticles are under a magnetic force for a given time. The absence of aligned nanochains until complete drying of a drop consolidates the role of the substrate in the assembly process. In the case of a negatively charged surface, repulsive substrate−particle interactions result in hydrodynamic movement, which can be attributed to attractive interactions between the identically charged NPs.[41] As a result, NPs aggregate into clusters on the surface. The aggregated structure of NPs could be governed by the effective charge density of the substrate, establishing the strength of the repulsive substrate−particle electrostatic force.[36,42] Consequently, modifying the strength of the surface charge of the substrate provides a simple route to regulating the nanochain dimensions. The assembly processes of NPs on bare glass are clearly revealed in Video 2 (SI). Several seconds after application of the magnetic field, very short and thin, but oriented NCs are observed on the surface, after which the NCs grow continuously over time. After ∼2 min, NCs and their movement can be clearly observed, hence revealing the arrangement mechanism. The clusters form linear chains as a result of the competition between Brownian motion and dipolar interactions between clusters in the initial stage. Because of the limited microscope resolution, this step cannot be observed at the very beginning of Video 2 (SI). However, an AFM image of linearly formed NCs that were initially pinned to the substrate near the original perimeter of the droplet provides clear evidence (Figure S1A, SI). Consecutively, the preformed NCs interact mutually and coalesce as a result of long-range dipolar forces. Typically, NCs strongly attract or repulse each other if they are placed head-to-tail or side-to-side, respectively.[26] It is worth noticing that preformed NCs are confined to the two-dimensional space of the glass over which they slip. Interestingly, it can be observed from Figure 3B that NCs can arrange themselves in a head-to-tail orientation starting from a side-to-side positioning. This could be due to both the freedom of the NCs to slip over the surface and thermal movements. Needle-shaped NCs, which can be clearly seen in Figure 2A, Figure 2D (inset), and Figure S1B (SI), are a clue confirming the arrangement mechanism.

Figure 4B shows the binding energies between two Fe_3O_4@Au NPs calculated by the COMPASS force field. The binding energies of all of the investigated systems have positive values, indicating that, under a static magnetic field, attractive forces are expected between two Fe_3O_4@Au NPs. From Figure 4B, one can observe that the binding energy between two Fe_3O_4@Au NPs decreases with increasing distance between the two NPs, when the NPs are subjected to a static magnetic field. As described in our previous report,[16] control of the structure of self-assembled MPNCs can be obtained by adjusting the strength of the magnetic field, **B**. Accordingly, as the strength of the magnetic field increases, anisotropic structures are formed with increased dimensions because of the chain−chain aggregation process. Here, we experimentally studied the assembly of MPNCs using different concentrations of Fe_3O_4@Au NPs under a static magnetic field (Figure S3, SI). The experimental results agree well with the calculated results (Figure 4A). The diameter of the MPNCs increases from 130 to 620 nm as the concentration (decreased mean interparticle distance) of Fe_3O_4@Au NPs increases from 1 to 15 μg/mL. This result is attributed to the increased number of dipoles available for anisotropic structure generation with increasing colloidal concentration. The more dipoles (clusters, nanochains) there are, the more chances there are for cluster−cluster chaining and chain−chain aggregation.

The assembly of NPs at different temperatures was investigated to explore the influence of thermal dynamics. Figure S4 (SI) shows optical microscope images of MPNCs assembled at different temperatures. We found that there is an increase in the MPNC length for temperatures ranging between 300 and 305 K, followed by a continuous decrease until no MPNCs are observed (Figure 4C). As mentioned above, the alignment of clusters is primarily determined by vdW and dipolar forces. It is worth noticing that the ratio of the interaction energies (vdW, magnetic dipole) to the thermal energy (U/k_BT) is decisive for the formation of anisotropic

DOI: 10.1021/acsami.5b00904
ACS Appl. Mater. Interfaces 2015, 7, 8650−8658

MPNCs. Increased temperatures lower the ratio, which leads to a reduction of the dimensions of the MPNCs. However, the thermal particle motion was considered to be a novel driving force for chain coarsening (as mentioned previously).[43] Furthermore, we also calculated the binding energies between two Fe_3O_4@Au NPs as a function of temperature (Figure 4D). The results show that the binding energy exhibits a monotonic increase with increasing temperature. Therefore, there is an optimal temperature (305 K) at which length of the MPNCs reaches a maximum as a result of the balance between the thermal energy and the magnetic dipolar interactions. As the temperature is increased further, the thermal force gradually becomes predominant, assuring a strong disruption of the initial formation of nanochains. Once the thermal motions overcomes the dipolar forces $[U_{dd(cluster)}/k_BT \ll 3]$ ($U_{dd(cluster)}$ = dipole−dipole energy of cluster), no formation of anisotropic structures occurs.

3.3. Magnetic Properties of MPNCs. An initial magnetism-related investigation of MPNCs at room temperature was performed by MFM. The corresponding MFM phase image of isolated core−shell NPs clearly shows a negative contrast, which is associated with the NPs (Figure S5, SI). This negative contrast indicates an attractive force between the tip and the sample, which is consistent with the fact that the magnetic field from the MFM tip weakly magnetizes the particle, thereby causing an attractive interaction. After repeated scans, but with reversal of the tip magnetization, negative contrast was still observed. This demonstrates the superparamagnetism of the isolated NPs, which well matches the SQUID analysis. The MFM analysis of the MPNCs shows magnetic behavior similar to that of the NPs (Figure S5D, SI). A negative phase arising from the NCs is observed regardless of the magnetization direction of the tip.

VSM measurements were performed for a deeper investigation of the magnetism of the NPs and NCs. The blocking temperature (T_B) is an important parameter for studying the magnetic behavior of a system. For magnetic nanocrystal aggregates (≤10 nm), T_B can range between 130 and 300 K depending on control of the NP organization or the particle−particle distance.[44,45] Panels A and B of Figure 5 show the field-dependent magnetizations of bare Fe_3O_4 NPs and NCs, respectively. The field-dependent magnetizations of the NPs and NCs exhibit superparamagnetic behavior at room temperature, whereas at 10 K, they exhibit a clear ferromagnetic hysteresis loop. From the zero-field-cooled (ZFC) and field-cooled (FC) curves shown in Figure 5C, the blocking temperatures (T_B) of bare Fe_3O_4 NPs and their corresponding NCs were estimated to be 50 and 130 K, respectively. The increased T_B value of the Fe_3O_4 NCs can be explained as a consequence of magnetic dipolar coupling between NPs separated by a short space of a stabilizing layer.[44−46]

In the case of the Fe_3O_4@Au core−shell NPs, the field-dependent magnetizations for the NPs and MPNCs also exhibit superparamagnetic behavior at room temperature and a ferromagnetic hysteresis loop at 10 K (Figure 5D,E). As shown in Figure 5, there is an increase in T_B for the Fe_3O_4@Au NPs (130 K) compared to the bare NPs (50K), which reflects the decreased coupling of the magnetic moments as a result of the increased interparticle spacing of the magnetic cores after application of the Au coating.[47,48] Moreover, little difference compared with the structural change was observed in the T_B values of the core−shell NPs (130 K) and their corresponding NCs (140 K), which also reflects very weak coupling of the magnetic moments among the NPs (Figure 5F). The slight increase in T_B for the MPNCs can probably be attributed to the fact that the Au coating layer acts as a spacer (∼10 nm), thereby effectively suppressing the magnetic interactions between neighboring NPs.[49] In Figure 5C, the lack of overlapping ZFC and FC curves for the bare Fe_3O_4 NCs indicates that the largest coupling structures were blocked at 300 K. The high value of T_B and the broad peak of the ZFC plot are consistent with the large variation in the size distribution of the NCs. In contrast, the narrower width of the ZFC plot for the MPNCs represents increased ordering of the distribution of spin alignment, demonstrating uniform magnetic structures of the assembled core−shell NPs.

4. CONCLUSIONS

The structures, assembly mechanism, and magnetic properties of magnetoplasmonic nanochains driven by an external static magnetic field were investigated in which substrate−particle interaction, magnetic forces, and vdW interactions were found to play fundamental roles in the arrangement of the NPs. Magnetic studies indicated that, on one hand, the Au coating layer enhances the magnetic anisotropy in individual Fe_3O_4@Au NPs. On the other hand, the coating layer, acting as a spacer, dramatically decreases the magnetic dipolar interactions between neighboring core−shell NPs, which will be probably useful for further research on biomedical applications and device fabrication in the nanoscale regime.

■ ASSOCIATED CONTENT

Ⓢ Supporting Information

Calculation details, evidence of single linear chains of clustered and coalesced chains, schematic illustration of the molecular dynamics simulation, images of MPNCs at different particle concentrations and temperatures, MFM images of particles and chains, and optical microscope videos of the assembly process. This material is available free of charge via the Internet at http://pubs.acs.org.

■ AUTHOR INFORMATION

Corresponding Author

*E-mail: jaebeom@pusan.ac.kr.

Author Contributions

‡V.T.T. and H.Z. contributed equally to this work

Notes

The authors declare no competing financial interest.

■ ACKNOWLEDGMENTS

This study was supported by a grant from the Korea Healthcare Technology R&D Project (HI13C0862); funds from the Ministry for Health, Welfare & Family Affairs; and basic research funds (NRF-2013R1A1A4A01004637); and Basic Science Research Program through the National Research Foundation of Korea (NRF) funded by the Ministry of Education (2014R1A1A2007222).

■ REFERENCES

(1) Yuan, J.; Xu, Y.; Muller, A. H. One-Dimensional Magnetic Inorganic−Organic Hybrid Nanomaterials. *Chem. Soc. Rev.* **2011**, *40*, 640−655.

(2) Walker, M. M.; Kirschvink, J. L.; Chang, S. B.; Dizon, A. E. A Candidate Magnetic Sense Organ in the Yellowfin Tuna, *Thunnus albacares*. *Science* **1984**, *224*, 751−753.

DOI: 10.1021/acsami.5b00904
ACS Appl. Mater. Interfaces 2015, 7, 8650−8658

(3) Frankel, R. B.; Blakemore, R. P.; Wolfe, R. S. Magnetite in Freshwater Magnetotactic Bacteria. *Science* **1979**, *203*, 1355.
(4) Komeili, A.; Li, Z.; Newman, D. K.; Jensen, G. J. Magnetosomes Are Cell Membrane Invaginations Organized by the Actin-Like Protein MamK. *Science* **2006**, *311*, 242−245.
(5) Tripp, S. L.; Pusztay, S. V.; Ribbe, A. E.; Wei, A. Self-Assembly of Cobalt Nanoparticle Rings. *J. Am. Chem. Soc.* **2002**, *124*, 7914−7915.
(6) Faivre, D.; Fischer, A.; Garcia-Rubio, I. s.; Mastrogiacomo, G.; Gehring, A. U. Development of Cellular Magnetic Dipoles in Magnetotactic Bacteria. *Biophys. J.* **2010**, *99*, 1268−1273.
(7) Scheffel, A.; Gruska, M.; Faivre, D.; Linaroudis, A.; Plitzko, J. M.; Schuler, D. An Acidic Protein Aligns Magnetosomes along a Filamentous Structure in Magnetotactic Bacteria. *Nature* **2005**, *440*, 110−114.
(8) Lalatonne, Y.; Richardi, J.; Pileni, M. P. van der Waals versus Dipolar Forces Controlling Mesoscopic Organizations of Magnetic Nanocrystals. *Nat. Mater.* **2004**, *3*, 121−125.
(9) Kornig, A.; e; Winklhofer, M.; Baumgartner, J.; Gonzalez, T. P.; Fratzl, P.; Faivre, D. Magnetite Crystal Orientation in Magnetosome Chains. *Adv. Funct. Mater.* **2014**, *24*, 3926−3932.
(10) Da Gama, M. T.; Tavares, J. M. Strongly Dipolar Fluids at Low Densities. *J. Phys.: Condens. Matter* **2000**, *12*, A471.
(11) Ghosh, S.; Puri, I. K. Soft Polymer Magnetic Nanocomposites: Microstructure Patterning by Magnetophoretic Transport and Self-Assembly. *Soft Matter* **2013**, *9*, 2024−2029.
(12) Fleissner, G.; Holtkamp-Rotzler, E.; Hanzlik, M.; Winklhofer, M.; Fleissner, G.; Petersen, N.; Wiltschko, W. Ultrastructural Analysis of a Putative Magnetoreceptor in the Beak of Homing Pigeons. *J. Comp. Neurol.* **2003**, *458*, 350−360.
(13) Hanzlik, M.; Heunemann, C.; Holtkamp-Rotzler, E.; Winklhofer, M.; Petersen, N.; Fleissner, G. Superparamagnetic Magnetite in the Upper Beak Tissue of Homing Pigeons. *Biometals* **2000**, *13*, 325−331.
(14) Ku, J.; Aruguete, D. M.; Alivisatos, A. P.; Geissler, P. L. Self-Assembly of Magnetic Nanoparticles in Evaporating Solution. *J. Am. Chem. Soc.* **2010**, *133*, 838−848.
(15) Crespo, P.; de la Presa, P.; Marin, P.; Multigner, M.; Alonso, J. M.; Rivero, G.; Yndurain, F.; Gonzalez-Calbet, J. M.; Hernando, A. Magnetism in Nanoparticles: Tuning Properties with Coatings. *J. Phys.: Condens. Matter* **2013**, *25*, 484006.
(16) Tran, V. T.; Zhou, H.; Kim, S.; Lee, J.; Kim, J.; Zou, F.; Kim, J.; Park, J. Y.; Lee, J. Self-Assembled Magnetoplasmonic Nanochain for DNA Sensing. *Sens. Actuators B: Chem.* **2014**, *203*, 817−823.
(17) Mohammad, F.; Balaji, G.; Weber, A.; Uppu, R. M.; Kumar, C. S. Influence of Gold Nanoshell on Hyperthermia of Superparamagnetic Iron Oxide Nanoparticles. *J. Phys. Chem. C* **2010**, *114*, 19194−19201.
(18) Banerjee, S.; Raja, S. O.; Sardar, M.; Gayathri, N.; Ghosh, B.; Dasgupta, A. Iron Oxide Nanoparticles Coated with Gold: Enhanced Magnetic Moment Due to Interfacial Effects. *J. Appl. Phys.* **2011**, *109*, 123902.
(19) Zhou, H.; Kim, J.-P.; Bahng, J. H.; Kotov, N. A.; Lee, J. Self-Assembly Mechanism of Spiky Magnetoplasmonic Supraparticles. *Adv. Funct. Mater.* **2014**, *24*, 1439−1448.
(20) Zhou, H.; Lee, J.; Park, T. J.; Lee, S. J.; Park, J. Y.; Lee, J. Ultrasensitive DNA Monitoring by Au−Fe_3O_4 Nanocomplex. *Sens. Actuators B* **2012**, *163*, 224−232.
(21) Boal, A. K.; Frankamp, B. L.; Uzun, O.; Tuominen, M. T.; Rotello, V. M. Modulation of Spacing and Magnetic Properties of Iron Oxide Nanoparticles through Polymer-Mediated "Bricks and Mortar" Self-Assembly. *Chem. Mater.* **2004**, *16*, 3252−3256.
(22) Link, S.; El-Sayed, M. A. Size and Temperature Dependence of the Plasmon Absorption of Colloidal Gold Nanoparticles. *J. Phys. Chem. B* **1999**, *103*, 4212−4217.
(23) Daniel, M. C.; Astruc, D. Gold Nanoparticles: Assembly, Supramolecular Chemistry, Quantum-Size-Related Properties, and Applications toward Biology, Catalysis, and Nanotechnology. *Chem. Rev.* **2004**, *104*, 293−346.
(24) Halas, N. J.; Lal, S.; Link, S.; Chang, W.-S.; Natelson, D.; Hafner, J. H.; Nordlander, P. A Plethora of Plasmonics from the Laboratory for Nanophotonics at Rice University. *Adv. Mater.* **2012**, *24*, 4842−4877.
(25) Morimoto, H.; Maekawa, T. Cluster Structures and Cluster−Cluster Aggregations in a Two-Dimensional Ferromagnetic Colloidal System. *J. Phys. A: Math. Theor.* **2000**, *33*, 247.
(26) Bishop, K. J.; Wilmer, C. E.; Soh, S.; Grzybowski, B. A. Nanoscale Forces and Their Uses in Self-Assembly. *small* **2009**, *5*, 1600−1630.
(27) Faraudo, J.; Andreu, J. S.; Camacho, J. Understanding Diluted Dispersions of Superparamagnetic Particles under Strong Magnetic Fields: A Review of Concepts, Theory and Simulations. *Soft Matter* **2013**, *9*, 6654−6664.
(28) Donselaar, L. N.; Frederik, M.; Bomans, P.; Buining, P. A.; Humbel, B. M.; Philipse, A. P. Visualisation of Particle Association in Magnetic Fluids in Zero-Field. *J. Magn. Magn. Mater.* **1999**, *201*, 58−61.
(29) Ge, J.; Hu, Y.; Biasini, M.; Beyermann, W. P.; Yin, Y. Superparamagnetic Magnetite Colloidal Nanocrystal Clusters. *Angew. Chem., Int. Ed.* **2007**, *46*, 4342−4345.
(30) Xia, Y.; Nguyen, T. D.; Yang, M.; Lee, B.; Santos, A.; Podsiadlo, P.; Tang, Z.; Glotzer, S. C.; Kotov, N. A. Self-Assembly of Self-Limiting Monodisperse Supraparticles from Polydisperse Nanoparticles. *Nat. Nanotechnol.* **2011**, *6*, 580−587.
(31) Xia, Y.; Tang, Z. Monodisperse Inorganic Supraparticles: Formation Mechanism, Properties and Applications. *Chem. Commun.* **2012**, *48*, 6320−6336.
(32) Derjaguin, B. V. Theory of the Stability of Strongly Charged Lyophobic Sols and the Adhesion of Strongly Charged Particles in Solutions of Electrolytes. *Acta Physicochim. URSS* **1941**, *14*, 633−662.
(33) Verwey, E. J. W.; Overbeek, J. Th. G. *Theory of the Stability of Lyophobic Colloids*; Dover Publications: New York, 1999.
(34) Crocker, J. C.; Grier, D. G. Methods of Digital Video Microscopy for Colloidal Studies. *J. Colloid Interface Sci.* **1996**, *179*, 298−310.
(35) Larsen, A. E.; Grier, D. G. Like-Charge Attractions in Metastable Colloidal Crystallites. *Nature* **1997**, *385*, 230−233.
(36) Bowen, W. R.; Sharif, A. O. Long-Range Electrostatic Attraction between Like-Charge Spheres in a Charged Pore. *Nature* **1998**, *393*, 663−665.
(37) Zhang, D.; Gonzalez-Mozuelos, P.; Olvera de la Cruz, M. Cluster Formation by Charged Nanoparticles on a Surface in Aqueous Solution. *J. Phys. Chem. C* **2010**, *114*, 3754−3762.
(38) Sader, J. E.; Chan, D. Y. Long-Range Electrostatic Attractions between Identically Charged Particles in Confined Geometries and the Poisson−Boltzmann Theory. *Langmuir* **2000**, *16*, 324−331.
(39) Kobayashi, Y.; Takahashi, H.; Kouta, H.; Fujiwara, Y. Adsorption Enhancement of Pd and Ag Colloidal Catalysts for Electroless Cu Deposition Using Cationic Polylectrolytes. Presented at the *214th ECS Meeting*, Honolulu, Hawaii, Oct 12−17, 2008; Abstract 2522.
(40) Horan, F. E.; Hirsch, F. G.; Wood, L. A.; Wright, I. S. Surface Effects on Blood-Clotting Components As Determined by Zeta-Potentials. *J. Clin. Invest.* **1950**, *29*, 202.
(41) Squires, T. M.; Brenner, M. P. Like-Charge Attraction and Hydrodynamic Interaction. *Phys. Rev. Lett.* **2000**, *85*, 4976.
(42) Gomez, E. W.; Clack, N. G.; Wu, H. J.; Groves, J. T. Like-Charge Interactions between Colloidal Particles Are Asymmetric with Respect to Sign. *Soft Matter* **2009**, *5*, 1931−1936.
(43) Halsey, T. Electrorheological Fluids. *Science* **1992**, *258*, 761−766.
(44) Rumpf, K.; Granitzer, P.; Morales, P. M.; Poelt, P.; Reissner, M. Variable Blocking Temperature of a Porous Silicon/Fe_3O_4 Composite Due to Different Interactions of the Magnetic Nanoparticles. *Nanoscale Res. Lett.* **2012**, *7*, 1−4.
(45) Frankamp, B. L.; Boal, A. K.; Tuominen, M. T.; Rotello, V. M. Direct Control of the Magnetic Interaction between Iron Oxide

DOI: 10.1021/acsami.5b00904
ACS Appl. Mater. Interfaces 2015, 7, 8650−8658

Nanoparticles through Dendrimer-Mediated Self-Assembly. *J. Am. Chem. Soc.* **2005**, *127*, 9731−9735.
(46) Serantes, D.; Baldomir, D.; Pereiro, M.; Hernando, B.; Prida, V. M.; Llamazares, J. S.; Zhukov, A.; Ilyn, M.; Gonzalez, J. Magnetic Ordering in Arrays of One-Dimensional Nanoparticle Chains. *J. Phys. D: Appl. Phys.* **2009**, *42*, 215003.
(47) Kumar, C. S.; Mohammad, F. Magnetic Nanomaterials for Hyperthermia-Based Therapy and Controlled Drug Delivery. *Adv. Drug Delivery Rev.* **2011**, *63*, 789−808.
(48) Wang, L.; Wang, L.; Luo, J.; Fan, Q.; Suzuki, M.; Suzuki, I. S.; Engelhard, M. H.; Lin, Y.; Kim, N.; Wang, J. Q. Monodispersed Core−Shell Fe_3O_4@Au Nanoparticles. *J. Phys. Chem. B* **2005**, *109*, 21593−21601.
(49) Fleutot, S.; Nealon, G. L.; Pauly, M.; Pichon, B. P.; Leuvrey, C.; Drillon, M.; Gallani, J. L.; Guillon, D.; Donnio, B.; Begin-Colin, S. Spacing-Dependent Dipolar Interactions in Dendronized Magnetic Iron Oxide Nanoparticle 2D Arrays and Powders. *Nanoscale* **2013**, *5*, 1507−1516.

DOI: 10.1021/acsami.5b00904
ACS Appl. Mater. Interfaces 2015, 7, 8650−8658